High-Resolution Vibrational Inelastic Neutron Scattering: A New Spectroscopic Tool for Globular Proteins[⊥]

Anne V. Goupil-Lamy,[‡] Jeremy C. Smith,*[,‡] Junko Yunoki,[†] Stewart F. Parker,[§] and Mikio Kataoka[†]

Contribution from the SBPM/DBCM, CEA-Saclay, 91191 Gif-sur-Yvette Cedex, France, Department of Earth and Space Science, Graduate School of Science, Osaka University, Toyonaka 560, Japan, and ISIS Facility, Rutherford Appleton Laboratory, Chilton, Didcot, OX11 0QX, U.K.

Received April 29, 1997. Revised Manuscript Received July 23, 1997[⊗]

Abstract: Inelastic neutron scattering is a form of vibrational spectroscopy for which the measured scattering intensities are directly related to vibrational amplitudes, allowing, in principle, convenient comparison with theoretical dynamical models. However, until recently, neutron sources and instruments have not allowed spectra to be collected on globular proteins with useful energy resolutions in the frequency range of most macromolecular vibrations (∼50−3500 cm^{-1}). The construction of the time-focussing crystal analyzer (TFXA) spectrometer at the ISIS pulsed neutron source near Oxford has changed this situation, allowing high-resolution spectra to be obtained over the whole frequency range of interest. We present here TFXA vibrational spectra of the enzyme, Staphylococcal nuclease, and compare the results with spectra calculated from a normal mode analysis of the protein using the program CHARMM (see ref 1). The calculated spectral intensities, which were obtained using a force field that was not refined to fit the present experimental data, are in general agreement with experiment and are used to assign the peaks.

Introduction

Infrared and Raman optical spectroscopies are commonly used to probe the local structure and dynamics of biological molecules. However, these techniques suffer from the drawback that the theoretical description of optical spectral intensities is complicated by the need to determine not only the nuclear vibrational dynamics of the sample but also associated charge fluctuations.[2−4] In infrared spectroscopy induced dipoles and charge transfer effects need to be calculated, while in Raman scattering a knowledge of polarizability fluctuations is required.

The problem of computing charge fluctuations is absent in the analysis of inelastic neutron scattering (INS), a form of vibrational spectroscopy complementary to infrared and Raman. The scattered INS intensity is expressed as the dynamic structure factor, $S(\vec{Q},\omega)$, a function of the momentum transfer, $\hbar\vec{Q}$, and the energy transfer, $\hbar\omega$, between the neutrons and the vibrational modes of the sample. $S(\vec{Q},\omega)$ can be computed directly from a knowledge of the frequencies and atomic displacement vectors of a theoretical vibrational analysis,[5] and for this reason INS is particularly convenient for testing vibrational and molecular mechanics force fields.

The application of INS to proteins has suffered from the relatively low particle flux of neutron sources (typically 10^7 cm^{-2} s^{-1}, compared with 10^{12} cm^{-2} s^{-1} for optical sources) and the absence of instruments with useful energy resolutions extending over the full frequency range of oscillations in macromolecules. Until now, the main usefulness of INS has been in the characterization of low-frequency (<100 cm^{-1}), collective global vibrations in proteins.[8] As the scattered INS intensity is approximately proportional to the square of the vibrational amplitude, low-frequency modes produce strong INS intensity. Using a time-of-flight spectrometer at the Institut Laue−Langevin reactor in Grenoble, $S(\vec{Q},\omega)$ and the vibrational density of states were determined for the bovine pancreatic trypsin inhibitor[7] and have been compared with calculations from normal mode analyses (See refs 6−8) and molecular dynamics simulations[9,10] using molecular mechanics potential functions. The very lowest-frequency modes (<15 cm^{-1}) predicted by the normal mode calculations were not found to exist in the experimental spectra. In experimental work on myoglobin the vibrational density of states has also been derived.[11]

The construction of the TFXA time-focussing crystal analyser (TFXA) spectrometer at the ISIS spallation neutron source near Oxford has given a new lease of life to molecular vibrational INS.[12] This spectrometer combines relatively high flux with an energy resolution approaching that of optical spectroscopies over the entire range of fundamental vibrational frequencies in proteins. This opens the way for detailed comparisons with the results of dynamical calculations and optical spectroscopic experiments. Recently, TFXA spectra have been documented and interpreted for collagen[14] and peptides.[15−17] Here we

[†] Osaka University.
[‡] SBPM/DBCM.
[§] Rutherford Appleton Laboratory.
[⊥] Keywords: protein dynamics, molecular mechanics, inelastic neutron scattering, normal mode analysis, vibrational spectroscopy.
[⊗] Abstract published in *Advance ACS Abstracts,* September 15, 1997.

(1) Brooks, B.; Bruccoleri, R.; Olafson, B.; States, D.; Swaminathan, S.; Karplus, M. *J. Comp. Chem.* **1983**, *4*, 187−217.
(2) Krimm, S; Bandekar, J. *Adv. Prot. Chem.* **1986**, *38*, 183−383.
(3) Souaille, M; Smith, J. C. *Mol. Phys.* **1996**, *87*(6), 1333−1347.
(4) Moeller, K. D; Williams, G. P.; Steinhauser, S.; Hirschmugl, C.; Smith. J. C. *Biophys. J.* **1992**, *61*, 276−280
(5) Zemach, A. C.; Glauber, R. J. *Phys. Rev.* **1956**, *101*, 118−129
(6) Smith, J. C.; Cusack, S.; Pezzeca, U.; Brooks, B.; Karplus, M. *J. Chem. Phys.* **1986**, *85*(6), 3636−3654.
(7) Smith, J. C.; Cusack, S.; Tidor, B.; Karplus, M. *J. Chem. Phys.* **1990**, *93*(5), 2974−2991.
(8) Smith, J. C. *Q. Rev. Biophys.* **1991**, *24*(3), 227−291.
(9) Hayward, S.; Kitao, A.; Hirata, F.; Go, N. *J. Mol. Biol.* **1993**, *234* 1201.
(10) Becker, O. M.; Karplus, M. *Phys. Rev. Lett.* **1993**, *70*, 3514.
(11) Cusack, S.; Doster, W. *Biophys. J.* **1990**, *58*, 243−251.
(12) Penfold, J.; Tomkinson, J. *Report RAL-86*−019; Rutherford-Appleton Laboratory: Chilton, UK, 1986.
(13) MacKerell, A. *et al.* Submitted for publication.
(14) Middendorf, H. D.; Hayward, R. L.; Parker, S. F.; Bradshaw, J.; Miller, A. *Biophys. J.* **1995**, *69*, 660−673.

S0002-7863(97)01364-4 CCC: $14.00

present the results of an experiment using TFXA on the vibrational neutron spectrum of a globular protein, the enzyme Staphylococcal nuclease (SNase). The experimental spectrum is compared with $S(\vec{Q},\omega)$ computed from a normal mode analysis of this protein performed in its full configurational space using the CHARMM molecular mechanics program.[1] The normal modes were computed using a potential function and parameter set that were not adjusted to fit the measured spectrum. Nevertheless, the form of the calculated scattering profile is found to be in reasonable agreement with experiment and allows the assignment of most of the observed vibrational peaks.

Methods

Experimental. Sample Preparation. Staphylococcal nuclease was expressed in Escherichia coli[18] and isolated. Transformed cells were a kind gift from Professor David Shortle at Johns Hopkins University School of Medicine. The protein was purified by urea extraction, ethanol precipitation, and ion-exchange chromatography with a pre-extraction step using 6 M urea.[19] The final eluate was dialyzed against pure H_2O and lyophilized. The lyophilized powder was dissolved into D_2O and relyophilized. This procedure was repeated two to three times to ensure complete exchange of the labile hydrogen atoms to deuterium. The final water content of lyophilized SNase is estimated to be between 3 and 5% of the weight. The powder (423 mg) was used as the specimen for the neutron experiment.

Neutron Experiments. The samples were contained in aluminum cells. The final neutron energy was 3.95 meV. Spectra were acquired at a single scattering angle of 135^o. The TFXA spectrometer utilizes the full white beam, achieving an energy resolution of between 1.4 and 4.5% of the energy transfer in the backscattering geometry used. The resolution function is as follows

$$\delta E = 16.7\,(\hbar\omega)^{-1/2} + 0.0006\,(\hbar\omega)^{3/2} \qquad (1)$$

This energy resolution is ~3% in the low-frequency region, decreasing to 1.4% between 200 and 300 cm^{-1} and then increasing to values between 3 and 4% in the 3000−4000 cm^{-1} range. A complete description of the experimental arrangement for TFXA can be found in ref.[12]

As a consequence of the conservation equations for energy and momentum, the scattering geometry for TFXA imposes the relation

$$Q^2 = 3.813 + \sqrt[2]{0.2287\omega + 7.27} + 0.06\omega \qquad (2)$$

where Q^2 is in Å^2 and ω in cm^{-1}.[12] The raw data from each detector were normalized to the incident neutron flux. In the scattering geometry used on TFXA multiple scattering and absorption are negligible and were neglected.

Theoretical. Normal Mode Calculations. The dynamical calculation was performed on the isolated SNase molecule, using the CHARMM program[1] with version 22 of the all-atom potential function and parameters.[13]

The potential energy function employed in all the calculations has the following form:

$$\left.\begin{aligned} V = &\sum_{\text{bonds}} k_b(b-b^0)^2 + \sum_{\text{angles}} k_\theta(\theta-\theta_0)^2 + \\ &\sum_{1:3} k_u(u-u_0)^2 + \sum_{\text{dihedrals}} k_\phi(1+\cos[n\phi-\delta]) + \\ &\sum_{\text{impropers}} k_\omega(\omega-\omega_0)^2 + \sum_{i,j} 4\epsilon_{ij}\left[\left(\frac{\sigma_{ij}}{r_{ij}}\right)^{12} - \left(\frac{\sigma_{ij}}{r_{ij}}\right)^{6}\right] + \\ &\sum_{i,j} \frac{1}{4\pi\epsilon}\frac{q_i q_j}{r_{ij}} \end{aligned}\right\} \qquad (3)$$

The function includes bonded interactions, comprising bond stretches, bond angle bends, and dihedral angle contributions, and nonbonded interactions between pairs (i,j) of atoms. In eq 3 b, u, θ, and ω are the bond lengths, Urey−Bradley 1:3 distances, angles, and improper dihedral angles in any given configuration and b_0, u_0, θ_0, and ω_0 are the reference values for these properties; the associated force constants are k_b, k_u, k_θ, and k_ω. The improper dihedral contributions are used to represent out-of-plane deformations of the sp^2 groups. For the intrinsic dihedral angles ϕ, k_ϕ is the force constant, n is the symmetry number of the rotor, and δ is the phase angle. The nonbonded interactions are included between pairs i,j of atoms on different molecules and on the same molecule separated by three or more bonds. They consist of a Lennard-Jones term, with parameters $\epsilon_{i,j}$ and $\sigma_{i,j}$ and a Coulombic electrostatic term between partial charges q_i, q_j.

The dielectric constant, $\epsilon = \epsilon_0 \cdot \epsilon_r$ was set to $\epsilon = \epsilon_0$, *i.e.*, $\epsilon_r = 1$. The electrostatic interaction energy was reduced by a factor of 0.5 for atoms separated by three bonds. Hydrogen bonds are described by the nonbonded terms in the energy function. All the interatomic electrostatic interactions were included *i.e.*, without long-range smoothing or truncation. Pairs of atoms on the same molecule separated by only two bonds may interact *via* a Urey−Bradley term harmonic in the distance between atoms i, j.

Crystallographic heavy-atom coordinates were taken from the Protein Data Bank entry 1STN.[20] Missing residues 1−6 and 142−149 were constructed as described in a previous paper[21] and the hydrogens added using the HBUILD routine of CHARMM. A second model of the protein was constructed by replacing the exchangable hydrogens with deuteriums. The models, each containing 2395 atoms, were energy-minimized using 8828 steps of the Adopted Basis Newton Raphson routine of CHARMM to an RMS gradient < 10^{-7} kcal/mol/Å. The RMS deviation of the backbone non-hydrogen atoms from the crystal structure was 1.7 Å.

The normal mode analyses were performed on the energy-minimized structures, by diagonalization of the mass-weighted second-derivative matrices. The analysis resulted in 7185 modes, six of which had zero frequency and represented translational and rotational degrees of freedom. Assignment of the calculated modes was effected by examining their potential energy distributions (for modes with ω > 1500 cm^{-1}) and by graphically inspecting dynamical trajectories created from the normal modes (for modes with ω < 1500 cm^{-1}).

The Dynamic Structure Factor, $S(\vec{Q},\omega)$. Neutrons are scattered by the nuclei of the sample. The inelastic scattering process probes time-dependent correlations of nuclear positions.[22] The dynamic structure factor, $S(\vec{Q},\omega)$, is a sum over

(15) Fillaux, F.; Fontaine, J. P.; Baron, M. H.; Kearley, G. K.; Tomkinson, J. *Chem. Phys.* **1993**, *176*, 249−278.
(16) Baudry, J.; Hayward, R. L.; Middendorf, H. D.; Smith, J. C. *J. Biomol. Struct. Dyn.* In press.
(17) Hayward, R. L.; Middendorf, H. D.; Wanderlingh, U.; Smith, J. C. *J. Chem. Phys.* **1995**, *102*(13), 5525−5541.
(18) Shortle, D. *J. Cell. Biochem.* **1986**, *30*, 281−289.
(19) Alexandrescu, A. T.; Abeygunawardana, C.; Shortle, D. *Biochemistry* **1994**, *33*, 1063−1072.
(20) Hynes, T. R.; Fox, R. O. *Proteins: Struct, Funct. Genetics.* **1991**, *10*, 92−105.
(21) Lamy, A.; Smith, J. C. *J. Am. Chem. Soc.* **1996**, *118*(31), 7326−7328.
(22) Lovesey, S. *Theory of Neutron Scattering from Condensed Matter*; International Series of Monographs on Physics. no. 72; Oxford Science Publications: Oxford, Clarendon, 1984.

all the atoms of the system of $S(\vec{Q},\omega)$ for each atom. $S(\vec{Q},\omega)$ may be written as a time Fourier transform of an intermediate scattering function $F(\vec{Q},t)$ as follows:

$$S(\vec{Q},\omega) = \frac{1}{2\pi}\int_{+\infty}^{-\infty} \mathrm{d}t\, e^{-i\omega t} F(\vec{Q},t) \quad (4)$$

$$F(\vec{Q},t) = \sum_{\alpha} b_{\alpha}^2 \langle e^{-i\vec{Q}\cdot\vec{R}_{\alpha}(0)} e^{i\vec{Q}\cdot\vec{R}_{\alpha}(t)}\rangle \quad (5)$$

α labels individual atoms whose positions are specified by their time-dependent position vector operators, $\vec{R}_{\alpha}(t)$. The brackets ⟨...⟩ indicate an equilibrium thermal average over the unperturbed states of the sample. The INS intensities are weighted by the scattering cross-sections of the nuclei and by the approximate amplitude of their motion. The scattering cross-section of the atom α is given by $b_{\alpha}^2 = b_{\mathrm{inc},\alpha}^2 + b_{\mathrm{coh},\alpha}^2$ where $b_{\mathrm{inc},\alpha}$ is the incoherent and $b_{\mathrm{coh},\alpha}$ is the coherent scattering length. Thus the calculations presented here include both incoherent and self-coherent scattering contributions. However, neutron scattering from proteins is dominated by incoherent scattering from the hydrogen atoms. This is largely because the incoherent scattering cross-section of hydrogen is 15 times greater than the total scattering cross-section of carbon, nitrogen, or oxygen. The amplitude-weighting of the scattered intensity leads to an even greater predominance of incoherent scattering from the hydrogen atoms, due to their smaller masses.

Neutron Scattering Intensities from a Harmonic Model. Under the assumption of harmonic dynamics the transform in eq 4 can be performed analytically and the result expanded in a power series over the normal modes of the protein. The following expression is obtained[5]

$$S(\vec{Q},\omega) = \sum_{\alpha} b_{\alpha}^2 \exp[-2W_{\alpha}(\vec{Q})] \prod_{\lambda} [\sum_{n_{\lambda}} \exp(n_{\lambda}\hbar\omega_{\lambda}\beta/2) \mathrm{I}_{n_{\lambda}}(X_{\lambda\alpha})] \delta[\omega - \sum_{\lambda} n_{\lambda}\omega_{\lambda}] \quad (6)$$

where

$$X_{\lambda\alpha} = \frac{\hbar(\vec{Q}\cdot\vec{e}_{\lambda\alpha})^2}{2m_{\alpha}\omega_{\lambda}\sinh(\hbar\omega_{\lambda}\beta/2)} \quad (7)$$

$W_{\alpha}(\vec{Q})$ is the exponent of the Debye−Waller factor, $\exp[-2W_{\alpha}(\vec{Q})]$, for atom α and may also be expressed as a sum over the modes

$$2W_{\alpha}(\vec{Q}) = \sum_{\lambda} \frac{\hbar(\vec{Q}\cdot\vec{\mathrm{e}}_{\lambda\alpha})^2}{m_{\alpha}\omega_{\lambda}} [2n(\omega_{\lambda}) + 1] = Q^2 \langle u_{\mathrm{Q}\alpha}^2\rangle \quad (8)$$

In eqs 6−8 m_{α} is the atomic mass, λ labels the mode, n_{λ} is the number of quanta exchanged with the mode λ, and $n(\omega_{\lambda})$ is the Bose occupancy. $\vec{e}_{\lambda\alpha}$ is the atomic eigenvector for atom α in mode λ, and ω_{λ} is the mode angular frequency. $\beta = 1/k_{\mathrm{B}}T$ where k_{B} is Boltzmann's constant and T the temperature. $\langle u_{Q\alpha}^2\rangle$ is the mean-square displacement for the atom α in the direction of the scattering vector $\vec{Q}$ and the brackets ⟨...⟩ again denote a thermal average.

$I_{n_{\lambda}}(X_{\lambda\alpha})$ is the n_{λ}th -order modified Bessel function. The small-argument approximation to this was used throughout the calculations:[6]

$$I_{n_{\lambda}}(X_{\lambda\alpha}) = \frac{1}{n_{\lambda}!}\left(\frac{X_{\lambda\alpha}}{2}\right)^{n_{\lambda}} \quad (9)$$

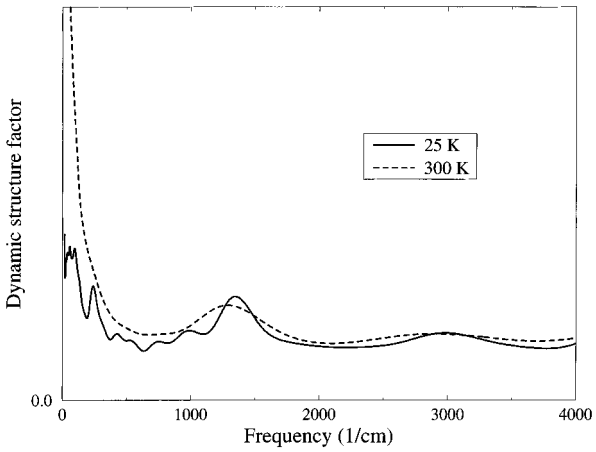

Figure 1. Experimental INS spectra of Staphylococcal nuclease at 300 and 25 K. The spectra have been smoothed for ease of comparison, by convoluting with a Gaussian function of half-width half-maximum 12% of the energy transfer. In this and Figure 2 the spectra have been separated on the $S(Q, \omega)$ axis for ease of visual comparison.

Equation 6 is an exact quantum-mechanical expression for the scattered intensity. It can be interpreted as follows. The Bose occupancies determine the energy distribution amongst the modes, ensuring that processes involving neutron energy gain are weaker than those involving neutron energy loss, in compliance with the quantum principle of detailed balance. In the present case the experimental data are neutron energy loss spectra, and the calculations are restricted to this part of the spectrum. The case where all of the n_{λ} equal zero corresponds to elastic scattering. The case where $\sum_{\lambda} n_{\lambda} = 1$ corresponds to single quantum processes, called one-phonon scattering. Two-phonon scattering is represented by terms in which $\sum_{\lambda} n_{\lambda} = 2$ *etc*. Higher order terms represent other multiphonon processes. Inserting the calculated eigenvectors and eigenvalues in eq 6 allows the calculation of the incoherent INS in the harmonic approximation to any degree in the phonon expansion. The present calculations were performed in the one-phonon approximation, *i.e.*,

$$S(\vec{Q},\omega) = \sum_{l=1}^{N} \sum_{\lambda=1}^{3N-6} b_{\alpha}^2 e^{\hbar\omega_{\lambda}\beta/2} \frac{e^{-2W_{\alpha}(\vec{Q})}\hbar|\vec{Q}\cdot\vec{e}_{\lambda\alpha}|^2}{4m_{\alpha}\omega_{\lambda}\sinh\left(\frac{\beta\hbar\omega_{\lambda}}{2}\right)} \delta(\omega - \omega_{\lambda}) \quad (10)$$

Equation 10 represents the full quantum-mechanical scattering function for the one-phonon scattering. To simulate the scattering from a typical experimental sample $S(\vec{Q},\omega)$ was averaged over three orthogonal directions of the molecular frame with respect to the scattering wavevector.

Results

In Figure 1 the experimental dynamic structure factors at 25 and 300 K are presented. The low-temperature spectrum is found to contain much more information (more structure) than the profile at 300 K. This is due in part to the Debye−Waller factor exponent, $W_{\alpha}(Q)$, which varies as Q^2/T. As, for TFXA, $Q^2 \sim \omega$ from eq 2, the intensity at high frequencies and temperatures is expected to be relatively low. The broadness of the spectrum at 300 K will also reflect anharmonic and multiphonon effects. At 300 K at low frequencies ($\omega < 500$ cm^{-1}) $S(Q, \omega)$ has a $\sim 1/\omega^2$ dependence, as was predicted from normal mode calculations on the bovine pancreatic trypsin inhibitor.[6]

Collecting the data at very low temperatures, *e.g.*, 25 K, reduces the mean-square atomic displacements, $\langle u^2_{\alpha,Q}\rangle$ and thus the Debye−Waller factor exponents ($W_\alpha(Q) \sim \langle u^2_{Q\alpha}\rangle\ Q^2$), leading to higher intensity at high frequencies relative to at low frequencies. Moreover, at 25 K the harmonic approximation to the potential surface, required for the normal mode calculations, is more accurate and frictional damping effects reduced, narrowing the INS peaks. Therefore, in what follows the comparisons between theory and experiment will be made at 25 K.

In Figure 2 the experimental and theoretical dynamic structure factors are presented. In Figure 2a the experimental data are compared with the theoretical spectrum represented as Kronecker δ-functions, one per mode, with amplitudes proportional to the one-phonon scattering function, calculated using eq 10. The spectra in Figure 2b are smoothed to enable comparison of the general features.

Detailed comparison with experiment should be made using Figure 2c, in which the experimental spectrum is compared with the theoretical one-phonon scattering function convoluted with the experimental resolution function. As the vibrational density of states is not uniform the Kronecker δ-functions are not evenly spaced on Figure 2a. Figure 2c takes into account this unevenness in the density of states. For example, as there are many more modes around 1350 than 1250 cm^{-1}, the resolution broadening leads to higher intensity in this region compared to the calculated spectrum in Figure 2a.

A number of peaks are present in the theoretical and experimental INS spectra. High-intensity bands in the experimental spectrum in Figure 2b are found at ∼2980, at ∼1340, and at ∼240 cm^{-1}. Other peaks can be identified at ∼990, ∼750, ∼420, and ∼550 cm^{-1}. At lower frequencies (<250 cm^{-1}) the dynamic structure factor is also intense. Most of the measured bands are also present in the calculated spectrum. However, some clear differences between experiment and theory do exist. One is in the position of the intense peak at ∼240 cm^{-1} which is found in the theoretical spectrum at 276 cm^{-1}. Another difference is in the shape of the massif at ∼1350 cm^{-1} in the experimental spectrum on Figure 2b. Comparison in Figure 2c shows that the intensity of the theoretical peak at ∼1290 cm^{-1} is somewhat too low. A further difference exists at ∼520 cm^{-1} where a peak is visible experimentally but is absent in the calculations. This frequency coincides with the water molecule rotational band that is visible in pure water in neutron scattering[23] and far-infrared spectroscopy.[24] It is possible that the small amount of remaining water in the lyophilized powder sample gives rise to this peak. Water molecules were not included in the normal mode analysis.

The experimental intensity between ∼1600 and ∼2800 cm^{-1} in Figure 2c is dominated by statistical noise. Low-intensity peaks are visible in the resolution-broadened theoretical one-phonon scattering function in this region but are below the experimental noise level. However, the intensity should in principle be nonzero in this region due to an approximately monotonic multiphonon scattering contribution, as illustrated in recent calculations up to the three-phonon level on a molecular crystal, acetanilide ($CH_3NHCOC_6H_5$, ACN).[17]

Differences between the theoretical and experimental spectrum in the region below 100 cm^{-1} are not significant as the experimental data suffer from poor counting statistics and low energy resolution. An analysis of neutron scattering by a small globular protein in this frequency range is given in ref 7.

(23) Teixera, J.; Bellissent-Funel, M.-C.; Chen, S.-H.; Dianoux, A. J. *J. Phys. Fr*. **1984**, Colloque C7. Suppl. 9 45−65.

(24) Hasted, J. B.; Husain, S. K.; Frescura, F. A. M.; Birch, J. R. *Chem. Phys. Lett.* **1985**, *118*, 622.

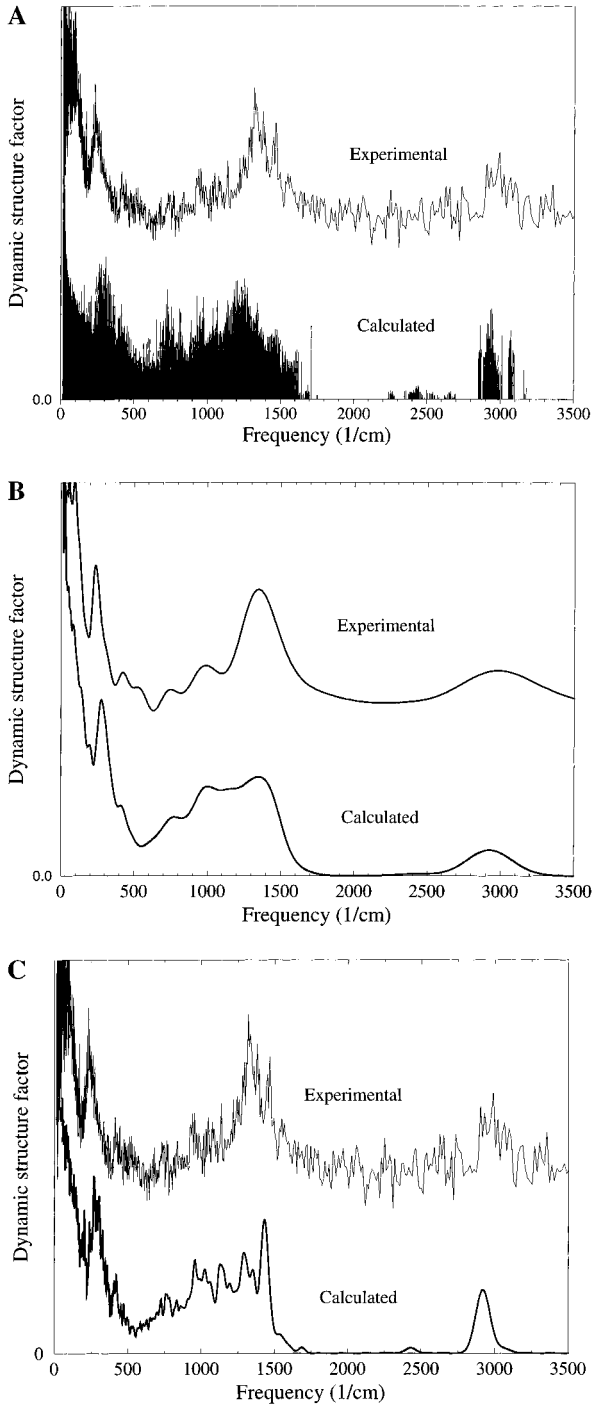

Figure 2. Experimental and theoretical inelastic neutron scattering spectra of Staphylococcal nuclease at 25 K. The theoretical scattering function includes the self-coherent and incoherent scattering from all the atoms in the protein, assuming complete exchange of the labile hydrogens for deuterium. (a) Corrected unsmoothed experimental spectrum together with theoretical one-phonon intensities represented as stick spectra (Kronecker delta functions) with intensities proportional to the dynamic structure factor. (b) As in Figure 2a except that the spectra are smoothed as in Figure 1 for ease of comparison of the major features. (c) As in Figure 2a except that the theoretical one-phonon spectrum is convoluted with the instrumental energy resolution function.

Examination of the displacement vectors of the modes giving rise to the theoretical INS peaks in Figure 2 showed that most of the peaks at ω < 1500 cm^{-1} do not arise from modes that can be simply described and contain contain contributions from many nondegenerate vibrations. However, it was possible to qualitatively identify some common features in the displacements contributing to many of the theoretical peaks. These are

Table 1. Frequencies (in cm^{-1}) of Vibrational Peaks in 25 K INS Spectrum from the TFXA Experiment and the Theoretical Normal Mode Analysis[a]

expt	theory	assignment
235	269	CH_3-t
400−450	395−435	CCC-def, CCN-def, skeletal
477	471	CCC-def, CCN-def, skeletal
470−590		water O-H..O- b
720−775	720−795	CH_2-r, CH-b
837	835	CH_2-r
936	958	CH_2-r, CH_3-r
1136	1136	CH-b, CH_2-tw, CH_3-r
1284	1291	CH_2-tw, CH_2-w, CH-b, CH_3-sb
1326		
	1352	CH_2-w, CH_2-tw, CH-b, CH_3-sb
1386		
1455	1431	CH_2-b, CH_3-ab, CH-ip
1555	1530	C-Ns
	1686	C-Ns
	2430	N-Ds
2952	2920	C-Hs

[a] Assignments of the theoretical modes are also given. For modes of frequency < 1500 cm^{-1} qualitative assignments were made by graphical inspection of dynamical trajectories. For each peak the order, from left to right, is in decreasing strength of the contribution. The abbreviations used are as follows: t = torsion; def = deformation; b = bend; r = rock; tw = twist; w = wag; sb = symmetric bend; ab = antisymmetric bend; ip = in-plane bend; s = stretch.

summarized in Table 1, in which the positions of the peaks in the calculated and experimental dynamic structure factor are also listed.

The stretch bands (>1500 cm^{-1}) were relatively easy to identify. The intense C−H stretch band is clearly visible at ∼2900 cm^{-1} in the experimental spectrum, and a C−N stretch is also present experimentally. Other stretch bands are present in the calculated spectrum but are below the experimental noise level. In the frequency range 1000−1500 cm^{-1} the strong intensity is due to vibrations that consist mostly of coupled angle deformations involving hydrogens (CH-b, CH_2-b, CH_2-w, CH_2-tw, CH_3-sb, CH_3-ab). The vibrations between 700−1000 cm^{-1} are mostly CH_3-r, CH_2-r, and C−C stretch.

In the low-frequency region some particularly clear spectral features are present. In the range 350−500 cm^{-1} the vibrations are delocalized over the protein and involve essentially coupled skeletal angle and dihedral displacements. These frequently involve backbone CCNC and side-chain CCCC degrees of freedom. The signal in this region is due primarily to the hydrogens riding on these skeletal displacements. The sharp peak at 235 cm^{-1} experimentally and 269 cm^{-1} theoretically is due to methyl torsions (CH_3-t). It is of interest to compare the present experimental value for the methyl torsional frequency with that previously documented in ACN.[17] In ACN the torsion is found at 145 cm^{-1} both experimentally and in a vibrational analysis of the crystal using the same form of potential function as in the present work. The rotational barrier associated with the ACN sp^2−sp^3 methyl torsion in the above theoretical analysis is ∼1 kcal/mol, significantly lower than that expected (∼3 kcal/mol) for the aliphatic sp^3−sp^3 methyl rotations in protein side chains. This is consistent with the higher torsional frequency observed in the present experiment.

The theoretical model can also be used to address problems concerning the effect of H−D exchange and the relative contribution of the hydrogen atoms to the measured intensity. In Figure 3 the hydrogen contribution to the total scattering function of the exchanged protein is shown. The hydrogen scattering dominates the theoretical spectrum, with the exception of the peak at 2400 cm^{-1} where the N−D stretch peak is visible. This peak is not observed experimentally because of the noise

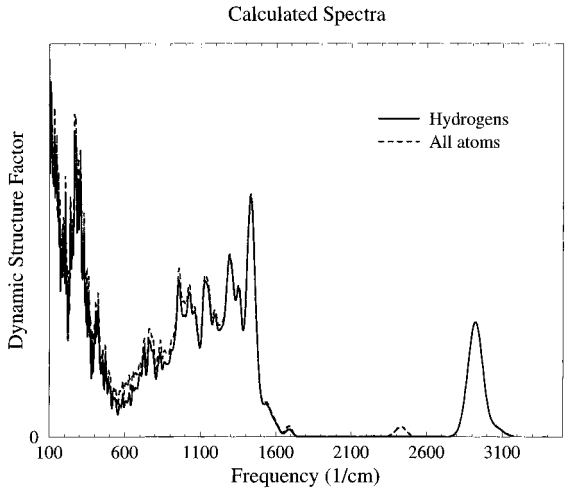

Figure 3. Effect of non-hydrogen atoms on the theoretical 25 K dynamic structure factor. The spectra are convoluted with the instrumental energy resolution function.

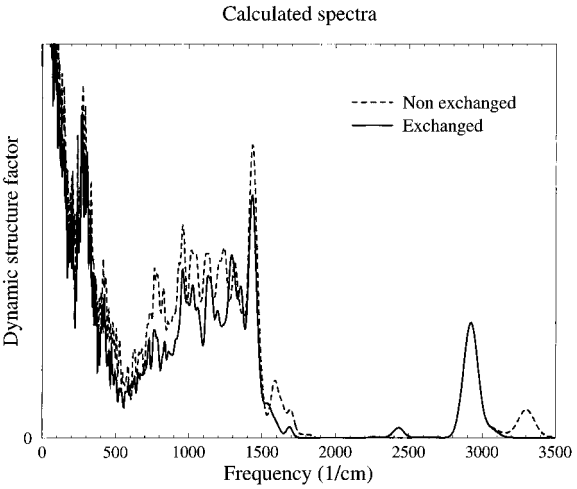

Figure 4. Effect of hydrogen−deuterium exchange on the theoretical 25 K dynamic structure factor. The spectra are convoluted with the instrumental energy resolution function.

present in this region. The non-hydrogen atoms do make a non-negligible contribution to the peak intensities at 500 < ω < 950 cm^{-1} and should be included in accurate comparisons of theoretical and experimental intensities in this region.

Finally, in Figure 4 the effect of hydrogen−deuterium exchange on the calculated spectrum is examined. Exchange of the labile protons shifts some of the peaks of the calculated spectrum, notably the N−H stretch at 3300 cm^{-1} that is displaced to the N−D stretch at ∼2430 cm^{-1}. The C−N stretch, at ∼1690 cm^{-1} in the nonexchanged protein, is also shifted to lower frequency and loses intensity. Exchange leads to about a 20% reduction in intensity in the region 700−1500 $cm.^{-1}$ This is mainly due to the fact that NH-ib, NH-ob, NH_2-b, and NH_2-r displacements contribute significantly to the spectrum of the nonexchanged protein in this region.

Conclusion

The work presented here demonstrates the potential of high-resolution INS spectroscopy for probing vibrations in globular proteins. The results demonstrate that 25 K spectra, as determined by TFXA, contain considerable structure.

The detailed interpretation of the observed peaks requires a theoretical analysis of the vibrations. This was performed in the present case using normal mode calculations with the

CHARMM program and associated molecular mechanics force field. The calculations provide a means of assigning the observed bands as well as of testing the accuracy of the force field. The theoretical spectrum, which was calculated using a force field that has not been adjusted to fit the neutron scattering data, is in general agreement with experiment. However, the agreement between experiment and theory is not perfect, and some improvements in the theoretical model can be envisaged. The methyl torsional barrier could probably be slightly reduced, so as to reduce the torsional frequency from 269 cm^{-1} to the observed value of 235 cm^{-1}. A closer agreement with experiment in other regions of the spectrum might require extra terms in the energy function. Moreover, refinements of the method of calculation of the scattering function (such as the explicit inclusion of multiphonon scattering) could also be envisaged. Improvements similar to the above were undertaken in the recent analysis of the TFXA spectrum of crystalline acetanilide.[17] The inclusion of bound water molecules in the SNase normal mode analysis might also produce improved agreement, particularly in the O−D···O hydrogen-bond bend region. The water content of the present sample is equivalent to about 40 water molecules per protein.

The dynamical calculations were performed in the harmonic approximation. The neglect of anharmonic contributions to the potential function is expected to lead to only small errors in the spectra. This is partly because the experiments and calculations were performed at 25 K, thus reducing atomic displacements relative to room temperature such that the atoms remain close to the bottom of their potential wells, and partly because the present analysis concerns mostly high-frequency vibrations ($\hbar\omega >> k_BT$) in which the harmonic, bonded terms in the potential function dominate. The reduced displacements will also reduce the multiphonon scattering contribution. Additional advantages to using the harmonic approximation, rather than molecular dynamics simulations with the full, anharmonic potential function, are that the quantum nature of the dynamical and scattering processes at low temperature are fully taken into account in the corresponding scattering functions, whereas the computation of the dynamic structure factor from classical trajectories presents considerable difficulties.

The present results indicate that the INS can now be exploited as a technique complementary to infrared and Raman spectroscopy for probing local vibrations in globular proteins—the complementarity arising from the absence of selection rules in INS and their presence in infrared absorption and Raman scattering. As shown here, INS also makes possible the direct comparison of intensity between experiment and theory. Despite these advantages, it is unlikely that in the near future that INS will become as commonly applied to proteins as the optical spectroscopies. This is due in part to the rarity of the appropriate neutron sources and instruments and the requirement of large amounts of sample (∼100 mg). A further limitation, at least as concerns TFXA, is the necessity to record spectra at very low temperatures. However, certain questions concerning the low temperature physical chemistry of proteins could well be addressed using this technique. For example, the existence of multiple minima on the potential surface will in principle lead to broadening of vibrational spectra that could be probed by careful comparison of experiment with theory.[25] Moreover, experiments designed at exploiting the large difference in scattering cross-section between hydrogen and deuterium may now be within reach and could yield information on local structure and dynamics in proteins. For example, a comparison of the exchanged and unexchanged proteins, examined here theoretically, can also be undertaken experimentally. Specific hydrogenation of selected residues of an otherwise fully deuterated protein might be a first step in this direction.

Acknowledgment. We thank the ISIS pulsed neutron facility for their assistance. The neutron scattering experiment was performed as part of the Japan−UK Collaboration Programme on Neutron Scattering. This work was supported partly by the grant-in-aid from the Ministry of Education, Science, Sports and Culture of Japan to M.K. The SNase mode frequencies and associated displacement vectors are available from A. L. at anne.lamy@cea.fr.

JA9713643

(25) Lamy, A.; Souaille, M.; Smith, J. C. *Biopolymers* **1996**, *39*,471−478.